LIQUIDICE

Deliverable 2.2 Snow water equivalent data set

eu-liquidice.eu

Funded by the European Union

Funded by the European Union. Views and opinions expressed are however those of the author(s) only and do not necessarily reflect those of the European Union or the European Climate, Infrastructure and Environment Executive Agency (CINEA). Neither the European Union nor the granting authority can be held responsible for them.

LIQUIDICE: LinkIng and QUantifying the Impacts of climate change on inlanD ICE, snow cover, and permafrost on water resources and society in vulnerable regions.

Funding programme: Horizon Europe
Project Start Date: 01.02.2025
Grant Agreement No.: 101184962
Duration: 48 months

Document information	
Work Package	2 -EO-based technologies for assessing the evolution of land ice and snow cover
Deliverable No.	2.2
Deliverable title	Snow water equivalent data set
Dissemination level	☒ PU - Public ☐ SEN - Sensitive
Lead Beneficiary	NORCE
Lead Author	Eirik Malnes
Contributors	NORCE
Contributing authors	Hannah Vickers, Robert Ricker, Tom Rune Lauknes
Due date	31.01.2026

Document history		
Version	1	
Version Date	30.01.2026	
Status	☒ Draft	07.01.2026
	☒WP leader approved	29.01.2026
	☒Coordinator approved	29.01.2026
	☒Executive Board / SST approved	30.01.2026

Table of contents

Executive summary

This report pertains to the Deliverable D2.2: Snow water equivalent data set, as described in ANNEX 1, part A (p. 32) of the EC/REA Grant Agreement for project number 101184962, "LIQUIDICE". Work Package 2 of the LIQUIDICE project is led by NORCE with the support of CNR, IISC, IITB, GEUS, UNIVBRIS, SIOS-KC and IG PAS. Other beneficiaries are also asked to contribute to the deliverable by reaching out to key people and organisations in each of their own countries.

The report provides a status for task 2.2 in LIQUIDICE. The task focus on measuring snow water equivalent using L-band SAR sensors. Since data from the NASA satellite NISAR was delayed in 2026, the task has focused on testing the retrieval method on ALOS-2 data. Additionally we investigate and discuss methods and datasets that can be used to validate the retrieval method and the products.

1. Introduction

1.1. Snow Water Equivalent

Snow Water Equivalent (SWE) has been a long-standing holy grail within the remote sensing community. This essential climate variable (ECV) contains the information about the total water content in a unit area of snow. In physical units SWE is the product of density and depth:

$$SWE = SD \times \frac{\rho_{snow}}{\rho_{water}}$$

Where SD is snow depth and ρ is the mass density of snow (100-350 kg/m^3 depending on the history of the snowpack) and liquid water (1000 kg/m^3). The SI-unit of SWE is meter [m], but frequently SWE is provided in mm. A typical SWE value for a snow cover of 1 m depth, is hence typically SWE=300 mm.

1.2. Satellite measurements

SWE has been measured with passive microwave sensors ranging back to 1986, but the spatial resolution of these products (~20km x20km) makes them impractical to use for many snow-covered areas, and in particular for mountainous regions where snow cover varies over much smaller spatial scales. Active radar sensors are hence needed for measuring SWE, and the requirement from WMO GCOS (https://gcos.wmo.int/) is that the parameter need to be measured with 500 m resolution. This requirement dictates that Synthetic Aperture Radars are needed. There exist several concepts in the literature for SWE measurements. These can roughly be grouped in two categories:

1) High-frequency SAR (X, Ku-band) where the backscatter difference between snow covered and snow free soil is used to derive SWE (Rott el al., 2010)
2) Low-frequency SAR (L-band, C-band) where the interferometric phase difference between snow covered and snow free soil is used. C-band (e.g. Sentinel-1 has been tested by several authors, but the concept is in practice useless since the decorrelation times are too short. L-band has been tested, with promising results (Nagler REF) but to a limited extend due to lack of L-band SAR data.

In LIQUIDICE we suggested to test out L-band SAR since this sensor type soon will become widely available on a global scale with the launch of NISAR (2025) and later with the operational ROSE-L two-satellite Copernicus constellation (2029). NISAR was launched in July 2025, and according to the current schedule, data will be released in March 2026, potentially including a backlog of acquisitions dating back to November 2025. If the backlog is also published it will allow SWE retrieval over LIQUIDICE study regions for the winter-season 2025/2026 and onwards.

1.3. In situ Measurements of snow water equivalent

Traditional measurements with depth soundings and density gauges have been described in (Stuefer et al., 2025). Snow depth can be measured using manual sounding sticks or with automatic equipment such as the Magnaprobe than log depth and position. Densities are measured using tubes with known volume either as snow bulk densities (entire snowpack down to ground) or samples of snow layers. These has typically been performed along transects of a few hundred m to a few km. Ground Penetrating Radars (GPR) mounted on snow scooters have taken over for manual measurements to some extent and can quantify both depth and SWE using

the two-way travel time from radar to ground below snow. GPR measurements can also be performed from drones (Jenssen &Jacobsen, 2021).

There are also some automatic measurement options for snow depth and SWE, but these are to a large extent point measurements, which makes them somewhat challenging to use as Fiducial Reference Measurements (FDR) for satellite retrieval of snow parameters as the representativeness of the in-situ stations seldom are documented.

Snow depth is frequently measured at meteorological stations using manual depth sticks, laser or acoustic equipment. These measurements are widely available from WMO (World Meteorological Organisation) and measured continually during winters, but they are a point measurement that very often is not representative for the surrounding area needed to compare them with remote sensing. Meteorological stations are also placed in urban environments where remote sensing can be challenging due to man-made structures.

Snow water equivalent can be measured using several instruments. The traditional snow pillows (flat sensor filled with antifreeze liquid that measures SWE by detecting the hydrostatic pressure exerted by the overlying snowpack) have been used for a few decades but are known to be hampered with large errors due to frost or ice bridges. Large scale snow weights have also been operated by some authorities (e.g. NVE). These have a large area (~2-5 m^2), which gives a better and more representative estimate of SWE than other types, but still not near the desired area (~100m^2) to match typical satellite resolutions. Another means of measuring SWE was recently introduced using fibre optic cables embedded in mats (Funnel & Thomas, 2023). These mats can cover the desired area, and there is ongoing project to quantify the accuracy. Other systems for SWE measurements are GNSS reflectometry and radiation-measurements (e.g. Gamma-sensors) that can use the background radiation and the absorption of the snowpack.

1.4. Work description

Below we cite the work package description for WP 2.2 SWE . *Improved snow water equivalent estimates for seasonal snow.*

Leading institute (NORCE), Contributing (IISc, India/IIT Bombay).

Snow water equivalent (SWE) contains crucial information on the snow amounts in a hydrological catchment but has so far not been possible to measure with sufficient accuracy in mountainous regions. L-band SAR sensors, capable of measuring SWE using interferometric (InSAR) techniques, will soon become available (NISAR from 2024 and ROSE-L from 2028). Methods will be developed based on InSAR techniques using multiple temporal baselines to compensate for loss of coherency during melting snow and variable TEC (total electron content in the ionosphere) which likely will affect the accuracy. Methods need to be validated with distributed SWE measurements (WP1) but technologies like ICESat-2 (Ice, Cloud, and land Elevation Satellite) sensitive to snow depth and access to data from hydropower companies could also be employed to assess accuracy for wider areas. SWE estimates will be provided for all catchments modelled in WP3 (Norway, Svalbard, Alps, Greenland and Himalayas) using NISAR data for the period 2025-2027.

2. SWE from L-band SAR (NORCE)

Due to the delayed launch of NISAR, there was no available L-band SAR data for the first year of LIQUIDICE. This was identified at the kick-off, and alternatives were discussed.

2.1. Data set

2.1.1. ALOS-2 data

Based on a JAXA EO-RA3 contract NORCE has 28 available ALOS-2 images from the period 13 May 2020 to 10 June 2023, sampled at 28 days interval (every second repeat pass). The product is a strip-map ultrafine image with 3 m spatial resolution in the HH-polarization. The incidence angle for flat terrain within the scene is 41°-45°.

Figure 1: Map over central parts of Spitsbergen with ALOS-2 image from 13 April 2022 superposed.

All SAR images are pre-processed to a Geotif-format using the inhouse software GSAR (Larsen et al., 2005). We used a 20 m digital terrain model (Moholdt et al., 2019) for terrain correction in the geocoding.

2.1.2. In-situ data

Data from the meteorological stations in Longyearbyen operated by The Norwegian Meteorological Institute has been used extensively to interpret results. Figure 2 shows a meteogram with temperature, precipitation and snow depth for two stations, Svalbard Airport and Reindalpasset, that had least and most snow, respectively. The winters 2021 and 2022 was similar in snow amounts. Interesting periods with avalanches, SWE-retrieval and rain-on-snow events have been marked.

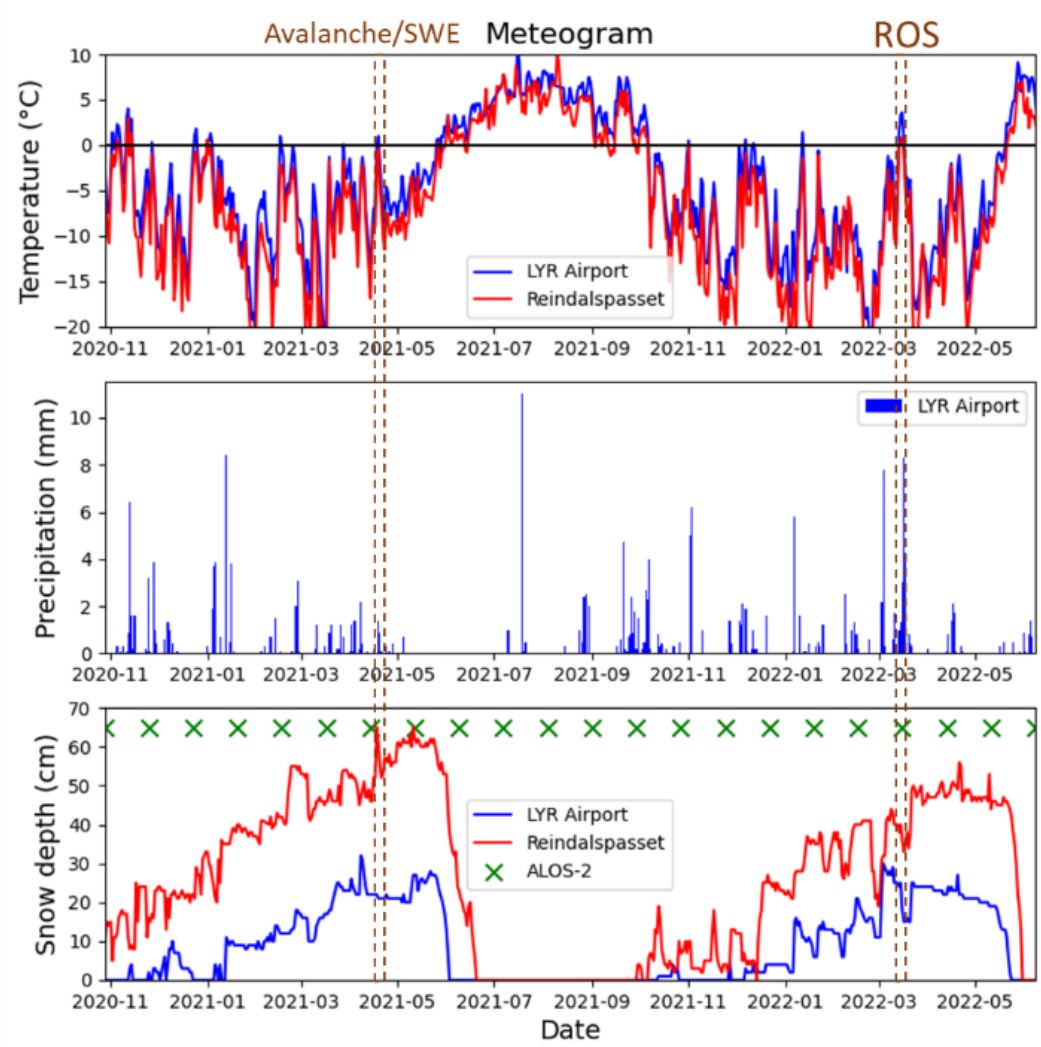

Figure 2. Meteogram (June 2020-June 2022) for Svalbard Airport and Reindalpasset. Times for ALOS-2 acquisitions (28 days intervals) are also indicated.

NORCE carried out snow related field campaigns in the area in April 2018-2022, and the results from these campaigns will be used for validation purposes. In the campaigns we measured snow profiles along transects using a Magnaprobe to validate snow profiles acquired using a drone-based ground penetrating radar instrument (Jensen &Jacobsen, 2021). Additionally, we also documented the snow stratigraphy using snow pits.

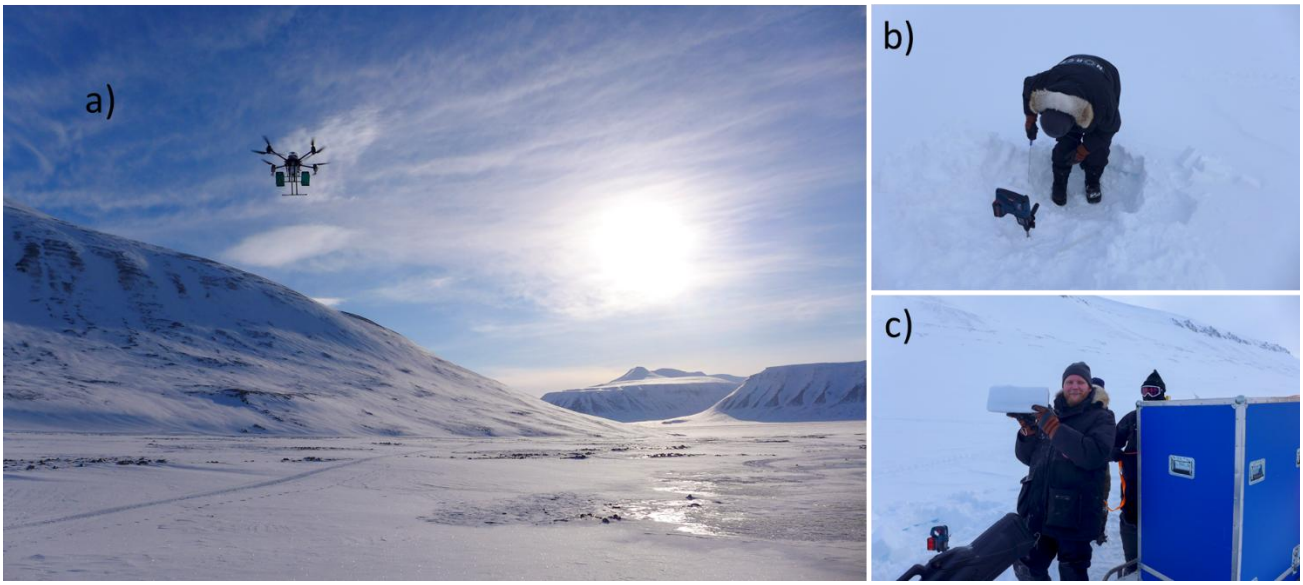

Figure 3. Field campaign photos 28.3-1.4.2022. a) Drone-mounted GPR operations, b) snow pit measurements, c) snow sampling.

2.2. InSAR SWE Measurement principle

Snow water equivalent for dry snow can be measured using repeat pass interferometry (Guneriussen et al., 2001) as the change in interferometric phase is proportional to the change in SWE (ΔSWE). C-band SAR, which has been the predominant SAR sensor since the launch of ERS-1 in 1991, has unfortunately limited capabilities mainly due to the rapid decorrelation at this frequency over snow cover. L-band SAR has higher coherency and longer unambiguous phase interval for a typical snowpack (16 cm for C-band vs. 74 cm for L-band). It is hence believed that with the launch of NISAR by NASA in 2025 and ROSE-L (by ESA/Copernicus in 2028) the SWE-retrieval technique finally can become operational.

As a first attempt to study the potential of L-band SAR for SWE retrieval we have hence processed the repeat pass interferograms for all the available ALOS-2 scenes in the data stack. We unwrapped the original interferogram phase.

Due to the difference in permittivity between air and snow, there is a change in path-length (or phase) when an interferogram is formed between to radar images from different snow depths. For dry snow Guneriussen et al. (2001) and Leins et al. (2015) showed that the phase change Δϕ between two repeat passes can be approximated to:

$$\Delta\phi = 4\pi / \lambda \cdot 1/2(1.59 + \theta\,\hat{}(5/2)) \cdot \Delta SWE \qquad (1)$$

where λ is the wavelength of the sensor (22.9 cm) and θ is the incidence angle of the radar (42°-44° for the current SAR scene).

Since the unwrapped interferograms contains a random, but on the spatial scale of our investigations, constant phase shift due to differences in the water column in the troposphere, movements in the ground and total electron content in the ionosphere, we need to subtract this effect. By modelling the phase as:

$$\phi = \phi\_ground + \phi\_snow + \phi\_atm + \phi\_iono \qquad (2)$$

The residual phase difference for two acquisition times t1 and t2 can now be estimated as:

$$\Delta\phi_0=\phi(t_2)-\phi(t_1) \qquad (3)$$

A recognized method to calculate this residual shift is by utilizing stable snow free corner reflectors, where we can assume that only the atmosphere and ionosphere components are variable. However, in our study area there were no such reflectors at the time of acquisitions. For this study, we thus chose to average the phase change over the airport landing stripe, that we assumed was snow free and with stable ground for the two acquisition times. For Svalbard airport we found that $\Delta\phi_0=1.6 \pm 2.4$ rad for the relevant period.

By substituting for the wavelength in eq (1) the change in SWE can be expressed as:

$$\Delta SWE=17.54\cdot(\Delta\phi-\Delta\phi_0) \quad [mm] \qquad (4)$$

Wet snow absorbs radio waves effectively and causes decorrelation of the interferometric phase. In this study we do not attempt to quantify SWE if snowmelt occurred.

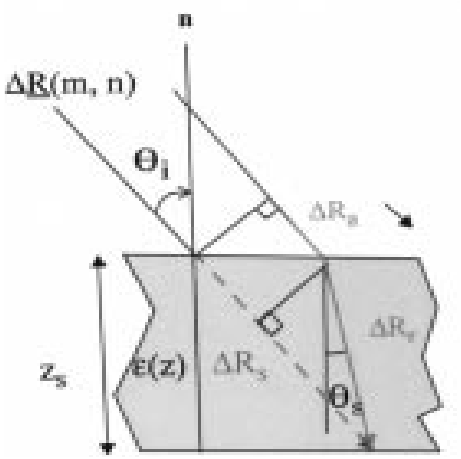

Figure 4 Geometry for repeat pass interferometric measurement of SWE (Guneriussen et al., 2001). Phase change due to increased SWE is related to refraction through the medium (snow) characterized by its permittivity. The change in phase $\Delta\phi$ or distance ΔR follows Snell's law for an oblique incidence angle θ .

2.3. SWE results in Adventdalen, Svalbard

Based on the methods described in section 2.1, we derive the change in SWE from all 27 interferograms (single pass) in the ALOS-2 time series. However, many of the interferograms were from time-intervals during summer periods with little snow (except at mountain peaks/glaciers) or melting snow, where the absorption due to liquid water in the snowpack also compromises the assumptions in the SWE retrieval method (eq. 1), In this study we therefore just analyze the results based on the interferogram formed from acquisitions on 17 February 2021 and 17 March 2021 (Figure 5), when we have a relatively stable snow period with temperatures below 0°C.

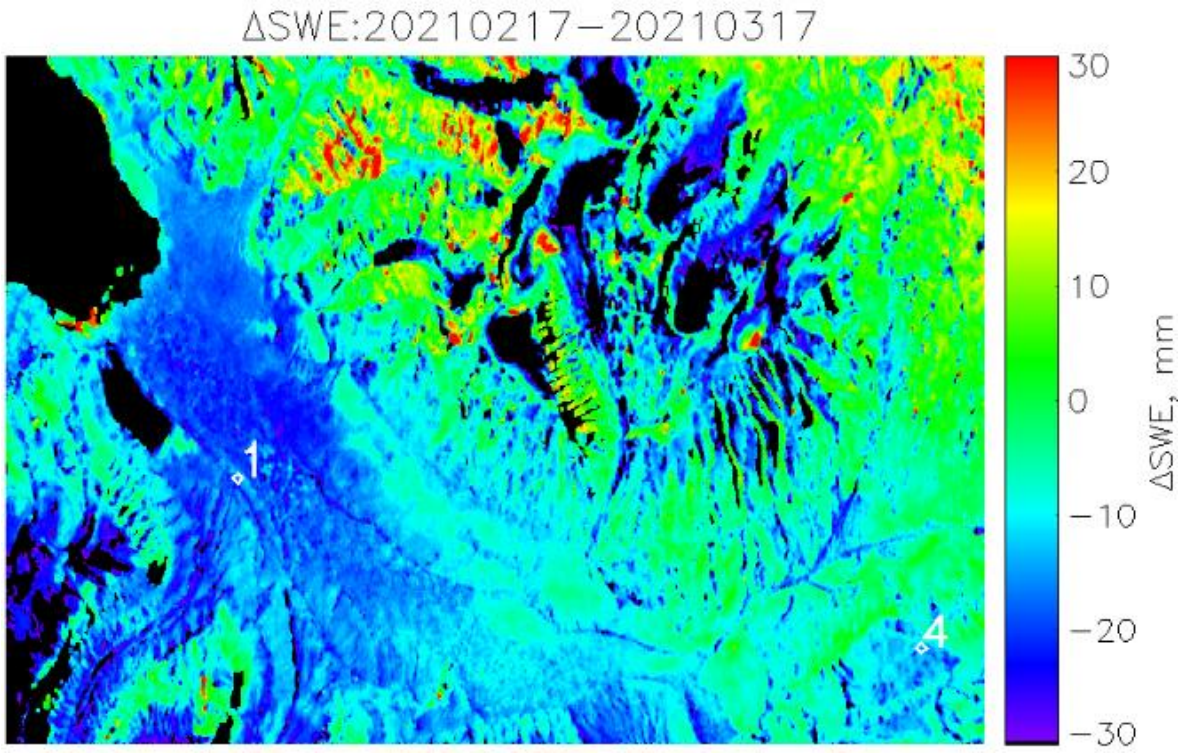

Figure 5: Estimated change in SWE for Adventdalen close to Longyearbyen for the time-interval 20210217-20210317. Black regions co-respond to masked areas (water and layo-ver/shadow). Meteorological stations are indicated as white diamonds.

Based on the ΔSWE-map in Fig 5 we see that the average change in SWE for the region in Adventdalen (lower right) for the time-interval is of the order -20 mm (blue).

2.4. Validation

For the same time interval (20210217- 20210317) we have also investigated the changes in snow depth for five meteorological stations located within the SAR scene (Table 1). We have also estimated the change in SWE for the same stations using the average snow bulk density of 0.3 km/dm3 (measured in the field campaigns on March 29, 2021). In Table 1 we have also calculated changes in SWE for the same positions in the ALOS-2 derived SWE data. The mean and standard deviation were calculated on a 5x5 grid centered around the locations to eliminate random errors.

Table 1. Changes in snow depth (Δsd) and SWE(ΔSWE) for 5 stations nearby Longyearbyen for the time interval 20210217 -20210317 and compared with changes measured by ALOS-2.

Stations	*Δsd met*	*ΔSWE met*	*ΔSWE,mm ALOS-2*
1. Adventdalen	-1 cm	-3 mm	-18±3 mm
2. Svalbard airport	+5 cm	+15 mm	+6±8 mm
3. Platåberget	+9 cm	+27 mm	-41±1 mm
4. Janssonhaugen	+3 cm	+9 mm	-13±9 mm
5. Reindalspasset	+4cm	12 mm	-17±7 mm

In Figure 6, we show snow depth transects and the distributions of snow measurements from the field campaign April 16, 2021, contrasted by snow depth estimates from March 17, 2021, derived

from satellite altimetry. NASA's Ice, Cloud, and land Elevation Satellite-2 (ICESat-2) was launched in 2018 and carries a laser altimeter that allows for detailed measurements of surface heights with a footprint of ~11 m, and 70 cm sampling along track (Magruder et al., 2020). During the summer season, in snow-free areas, ICESat-2 surface heights provide a refer-ence surface in combination with a high-resolution digital elevation model (Arctic DEM, Porter, Claire, et al., 2023). During winter, ICE-Sat-2 senses the snow surface, allowing estima-tions of snow depth when referenced to snow-free elevations.

Based on the averages from the two dates, the snow depth in the region increases by 7 cm, corresponding to 21 mm increase in SWE. Note that the date interval does not match the corresponding date interval for ALOS-2 (20210217 -20210317). The variability for each distribution is also high and can be attributed to the microtopography in the valley.

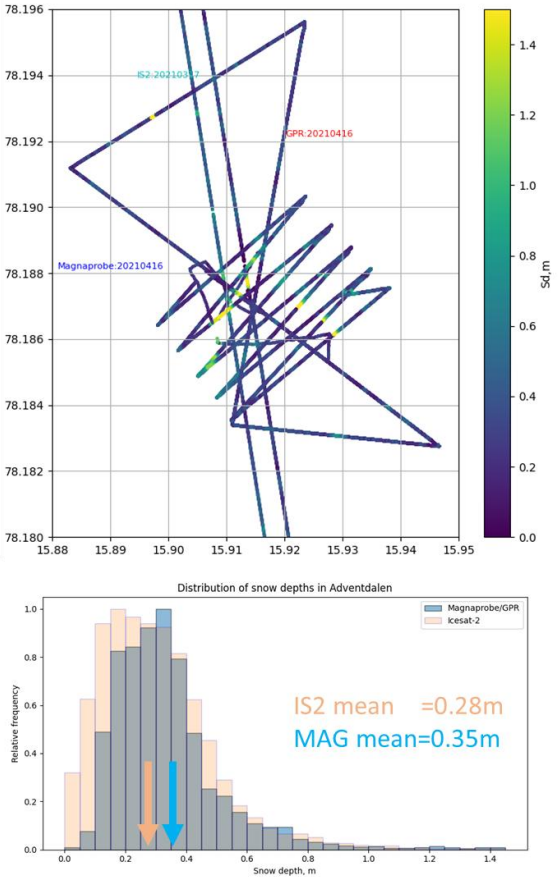

Figure 6. Top: Snow depth transects in Adventdalen 20210317 (ICEsat-2) and 20210416 (GPR/Magna-probe). Bottom: Distributions of snow depths from the transects.

2.5. Discussion

A preliminary analysis of the retrieval of changes in SWE was done for the dataset, but we have not studied the remaining interferograms for the entire period (May 2020-May 2022). This will be studied in upcoming work, but we chose to focus on a time-interval when field data was avail-able and the snow was dry, since melting snow most likely will cause loss of coherency.

The results are partially consistent with data from the meteorological stations in the region, but it is premature to conclude that the method is consistent. Comparing data from in situ meteorological stations (point-measurements) with remote sensing data (even at 3 m resolution) is very challenging since the point measurements often are not representative for the average snow depth in a region surrounding the measurements. Local microtopography and wind drift often control snow distributions at a very fine scale (see Fig 9). Ideally a validation should include distributed measurements of snow depth or SWE at both times of acquisitions. Alternatively, a larger snow weight could be used with more representative results.

2.5.1. Ionosphere correction

L-band SAR is highly sensitive to changes in the total electron content (TEC) in the ionosphere. The propagation of radar waves at L-band frequency will experience a significant change in the phase through the ionosphere that ultimately needs to be compensated. For a normal ionosphere this can be dealt with using TEC-maps provided by GPS-stations, but the ionosphere at high-latitudes is highly dynamic both spatially and temporally due to auroras produced by sun-storms. Future processing chains for SWE-retrieval using L-band SAR will have to deal with this effect on a systematic basis. In addition to the phase, it will also be important to study whether backscatter also can be modified through absorption in the ionosphere.

The geomagnetic activity in Longyearbyen (https://flux.phys.uit.no) for the relevant times was ~20 nT, as opposed to 300 nT, for disturbed conditions. The global Kp-index (provided by kp.gfz-potsdam.de) for the relevant days was 2.0 and 0.33 for 20210217 and 20210317, respectively. Kp=2.0 is not very high, but the difference between the two dates could be sufficiently high to produce a difference in TEC that change the interferograms. However, due to our calibration technique (averaging over the airfield to estimate the zero reference) should be sufficient to eliminate the spatial variabilities.

In contrast to C-band there is little need for InSAR corrections due to the water content in the troposphere in the interferograms. This type of correction may be regarded as secondary at this stage.

2.6. Conclusions and outlook

The method to retrieve snow water equivalent from L-band SAR data has been tested on ALOS-2 data over Svalbard. NISAR data will be available from winter 2025/2026.

3. SWE derived from ICESat-2 and CARRA (NORCE)

Snow cover in the High Arctic is a complex variable to monitor due to large variations in extent, amount (snow depth/SWE) and hence duration. The distribution of snow cover is affected on regional scales by weather systems bringing snowfall and their interaction with topography, while deposited snow can be redistributed on smaller scales by wind transport from exposed to more sheltered areas, which is a major driver of local scale variations in Svalbard, where there is little vegetation to inhibit the effects of wind transport. These variations in amount of snow and hence the timing of snow disappearance can further impact the ground surface temperature and soil moisture, thus leading to variations in nutrient availability with consequences for vegetation growth and terrestrial ecosystems. Modelling attempts to simulate these effects on snow cover and depth variability are not new and have been carried out for over 20 years (eg., Bruland et al.,

2004) with more recent studies extending the modelling to investigate the impact of snow cover variability on ground temperature (eg. Zweigel et al., 2021). SWE and bulk snow density are both common variables that can be estimated using snow models, but the different levels of complexities of snow models can result in varying levels of accuracy of these estimates within the model grid, which often have coarser resolution than typical scales of SWE and snow density variation. In this chapter we endeavor to evaluate altimeter-based estimates of snow depth (and SWE) against both reanalysis and snow model estimates.

3.1. ICESat-2 data from Svalbard

Svalbard, at 80° N, is experiencing the world's largest temperature anomaly linked to climate change. Rising air temperatures are rapidly altering the snow cover, yet the spatial distribution and volume of terrestrial snow in this high-Arctic environment remain poorly quantified. This knowledge gap stems from the scarcity of ground-based observation stations and, until recently, the limitations of satellite remote sensing in such conditions. The launch of ICESat-2 in 2018 introduced the capability to measure snow depth (SD) along laser altimeter transects, under cloud-free conditions. Within the SnowPilot project, we have retrieved snow depth data over three extended sites in Svalbard and compared them with available in situ measurements from manual surveys and ground-penetrating radar (GPR) transects. To overcome the limited temporal and spatial overlap between satellite and ground observations, we also validate ICESat-2 snow depth estimates against the Copernicus Arctic Regional Reanalysis (CARRA). This enables a triple-collocation approach, providing a robust assessment of snow depth from three independent sources: remotely sensed ICESat-2, in situ measurements, and CARRA.

3.2. Study area

Svalbard is located at 77-80º N, 11-27ºE. The study area encompasses 3 extended sites (~25x25 km) in the vicinity of the major research stations in Ny Ålesund, Longyearbyen and Hornsund. Snow depth has been retrieved from ICESat-2 transects for the years 2019-2025 over these 3 sites, but the retrievals are sparse due to the limited altimeter footprint and frequent cloud cover in Svalbard, and it is also spread out in time and space (see fig 1a). All data for the winter season (October-June) has been processed for the 5 years 2019-2025.

3.3. Method

All available ICESat-2 ALT03 level 2A data over the study sites was downloaded from NASA. The retrieval of snow depth is performed by subtracting a high-resolution digital terrain model (2m resolution) available over the study-sites from the instantaneous surface elevation measured by ICESat-2. Because of cloud cover and terrain steeper than about 10º being masked, the estimates are sparse and usually limited to up to six straight transects along the valley bottoms in Svalbard, corresponding to the six ICESat-2 beams. The sampling distance is typically 2-5 m and a ground footprint of the laser beam of with a diameter of 11m.

To validate the retrievals, we use in situ snow depth measurements from Magnaprobe-instruments, ground penetrating radars mounted on snowmobiles and drones, and daily snow depth measurements from meteorological stations. The field measurements were mainly carried out near snow depth maximum (March-April). We have also used data from the Copernicus service CARRA where snow depth has been derived using the snow density and snow water equivalent variables, to assess the snow depth data derived from ICESat-2. Lastly, we have used

the CARRA snow density variable to convert ICESat-2 snow depth to a SWE estimate using the relationship SWE = snow depth * snow density. An independent snow model dataset, seNorge, provides estimates of SWE for the entire Svalbard archipelago at 3-hourly intervals. We have utilised these estimates to evaluate the estimates of SWE made using a combination of ICESat-2 snow depth and CARRA snow density data

3.4. Results

In this chapter we report on results for snow depth and snow water equivalent based on ICESat-2 data and CARRA estimates for densities.

3.4.1. Snow depth from ICESat-2

Snow depth is highly variable in the complex terrain of Svalbard. Comparing SD retrievals from two measurements should ideally be done using measurements made only a few meters apart and with minimum time-lag. This is very challenging to achieve at Arctic sites as most in-situ datasets are field campaign-based. On some occasions we have carefully planned field campaigns to follow the pre-defined ICESat-2 tracks.

The validation results (Fig 7b) show that there is a fair correlation between in situ data and meteorological data against ICESat-2 retrieval of snow depths (bias 0.14 cm, standard deviation 25 cm), but this is highly dependent on how restrictive we are in masking matchups of in situ and ICESat-2 depending on proximity in space and time. Statistically, the distributions of snow depths from ICESat-2 and in situ measurements have a fair overlap.

CARRA data also provide a reasonable comparison statistically at Adventdalen (Fig 7c), but due to the relatively low resolution of CARRA (2.5km pixels) it is hard to evaluate the overall accuracy since each ICESat-2 transect samples a small part of each CARRA-pixel. However, when the ICESat-2 measurements are assigned the nearest grid cell in the CARRA grid, there can be up to several thousand measurements available for averaging and comparing with the CARRA snow depth. We find that using the grid cells with a higher number of ICESat-2 measurements used in averaging gives a higher correlation with CARRA overall. The temporal variability correlates well between CARRA and ICESat-2 retrievals.

ICESat-2 retrievals of snow depth is a valuable complementary dataset to in situ measurements of snow in a remote Arctic site like Svalbard. The dataset could play a crucial role in understanding the ongoing climate changes. Due to the intrinsic biases, sparseness and non-systematic sampling regime of ICESat-2, assimilation of ICESat-2 in high-resolution reanalysis products for snow depth is a challenging topic, but ongoing work using digital twin solutions based on AI could provide a viable path.

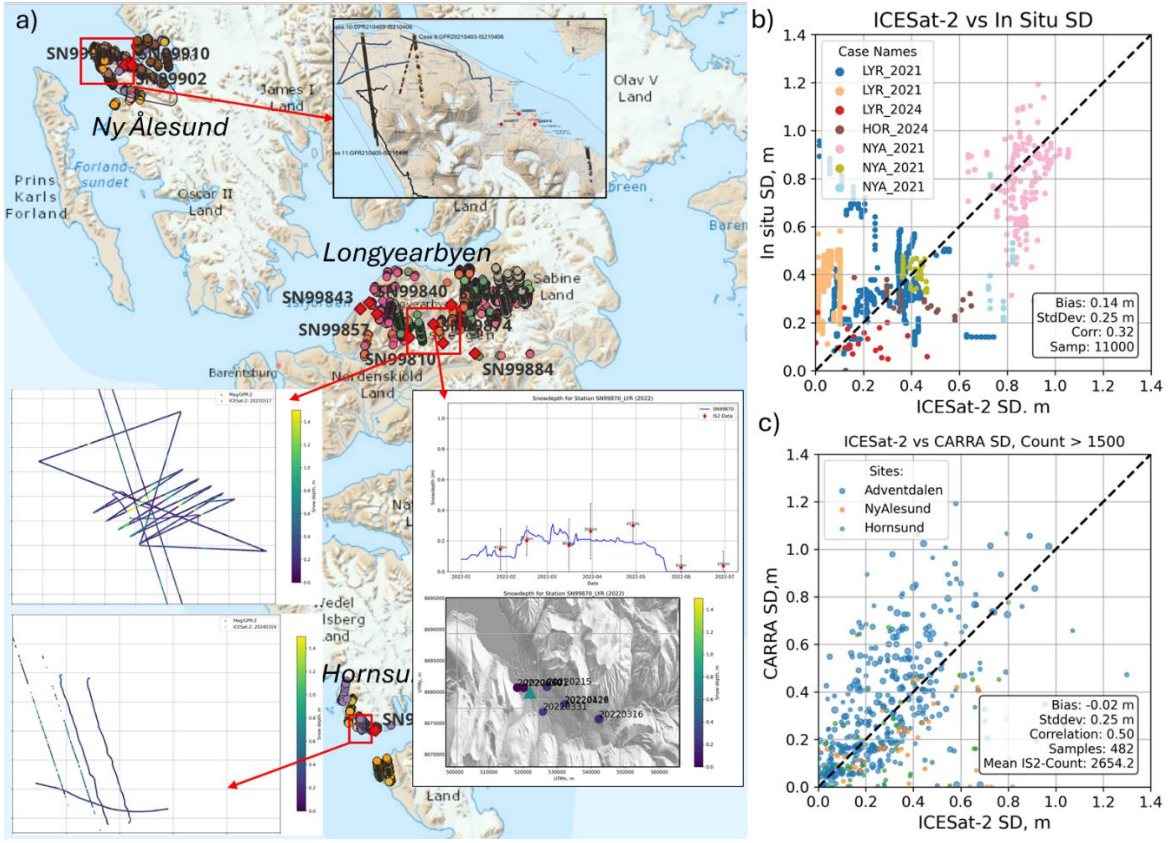

Figure 7 (a) map of study sites with Icesat-2 tracks and in situ measurements (with intercepts of concrete comparisons of individual campaigns and met-station data), (b&c) comparison ICESAT.2 vs in situ and CARRA estimates.

3.4.2. Snow depth from meteorological stations

Meteorological stations in Svalbard have measured snow depths since 1950, but the locations of the sites have changed over the years. Figure 8 shows the maximum snow depths per year for most of the meteorological stations that has operated since 1950. The number of stations (and geographical spread) have increased significantly since 1980, and then further increased about 2010-2020 with the introduction of automatic stations. The average snow depth is of order 55 cm, but it is challenging to state a clear climate trend due to the varying number of stations available.

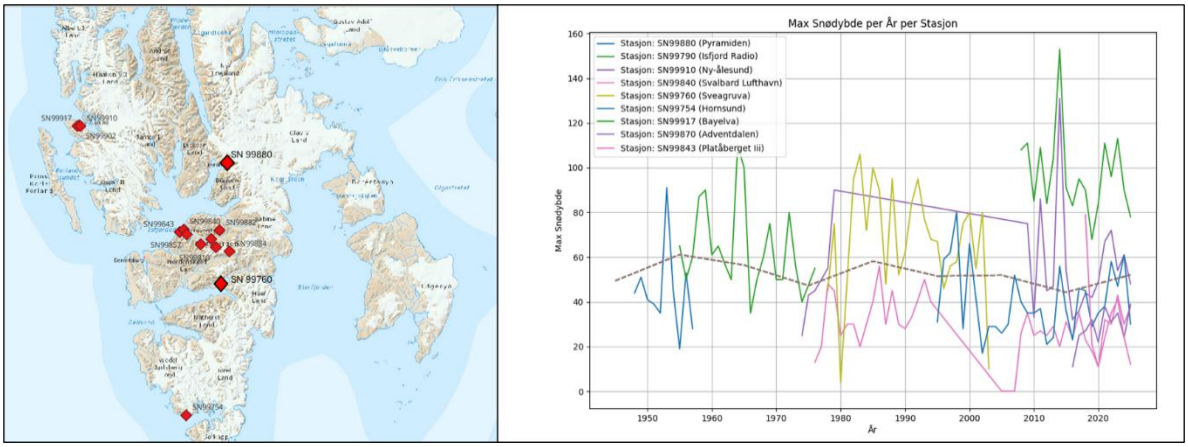

Figure 8. Locations of met stations in Svalbard (left) and annual maximum snow depth for the years the stations have operated (right).

3.4.3. Snow water equivalent estimates using ICESat-2 SD and CARRA density data

In Figure 9 we compare ICESat-2 snow depth estimates with CARRA snow depths.

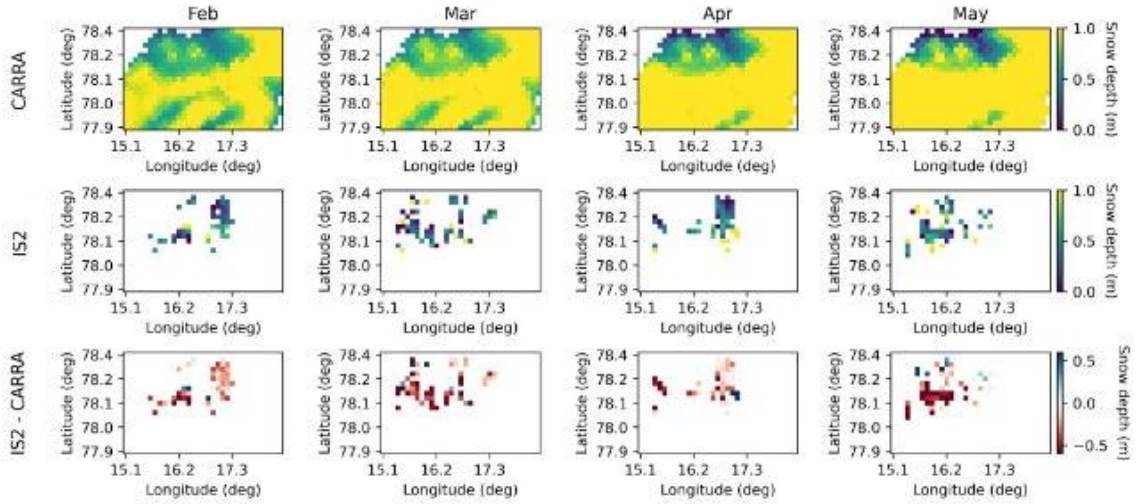

Figure 9. Snow depth averages for Feb-May 2024 from CARRA and Icesat-2 over Longyearbyen region.

To convert ICESat-2 snow depth to an estimate of SWE, we multiplied the mean snow depth calculated for a CARRA grid cell with the corresponding snow density from CARRA. The independent seNorge dataset provided 3-hourly estimates of SWE on a 1km x 1km grid, which were averaged to produce daily values. The seNorge data were then resampled to the CARRA grid to extract SWE estimates at the same grid spacing corresponding to those derived with a combination of ICESat-2 snow depth and CARRA snow density.

Figures 13 to 15 show a comparison of the ICESat-2 SWE and seNorge SWE estimates over Adventdalen, for the winters 2019/2020, 2020/2021 and 2021/2022. The data have been further filtered to show only the grid cells where there was a minimum of 1500 ICESat-2 measurements used to obtain an average snow depth for that grid cell. Negative values have also been filtered out. Here, it can be seen that there is a relatively strong and positive correlation between IS2 and seNorge estimates of SWE, with R ranging between 0.7 and 0.8, though with a slight bias towards lower SWE in seNorge compared to the IS2/CARRA-derived SWE estimates. Overall, the results indicate that IS2 snow depths, when combined with estimates of bulk snow density from reanalysis, can be used to estimate SWE in reasonable agreement with those derived from simple snow models. However, it should be emphasized that while snow models provide a source with which to evaluate the IS2 estimates against, they are by no means a ground truth.

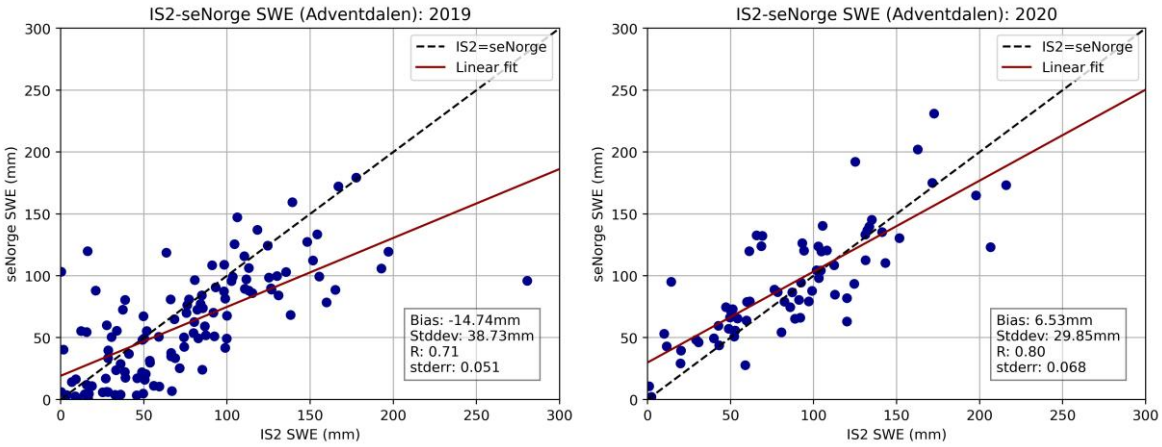

Figure 10 (left): seNorge SWE vs. IS2 SWE for Adventdalen from winter 2019/2020 and () (right): SWE estimates from seNorge and IS2 in winter 2020/2021

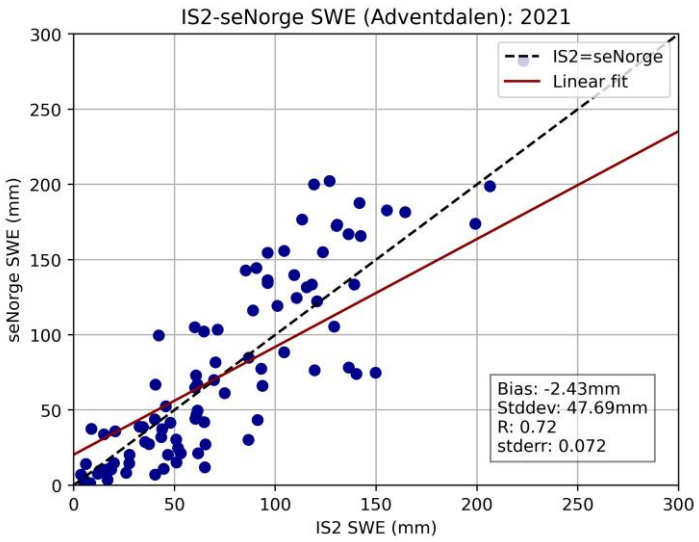

Figure 11: SWE estimates from seNorge and IS2 for Adventdalen for the 2021/2022 winter

Figures 10 and 11 show examples of the correlation between seNorge and IS2 SWE estimates made using data from Hornsund and Ny-Ålesund respectively. At these sites there were on average around three times fewer IS2 measurements of snow depth per CARRA grid cell compared to those made over Adventdalen, most likely due to the proximity of Hornsund and Ny-Ålesund to the coast, resulting in less land over which to derive snow depth estimates within the CARRA grid cell. Due to this issue a lower threshold of 500 measurements was used to filter grid cells with mean snow depth estimates from IS2. However, despite fewer data points being available at these sites, Figure 12 demonstrate that the same level of correlation and bias are observed at Hornsund and Ny-Ålesund as was obtained at Adventdalen, indicating consistency in the relationship between the seNorge and IS2 estimates across different sites.

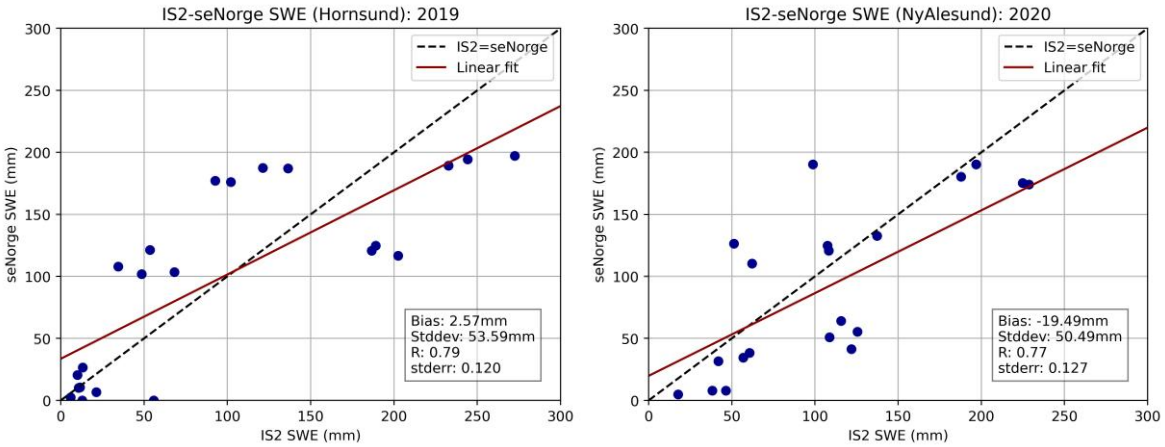

Figure 12 (left): seNorge SWE vs. IS2 SWE for Hornsund from winter 2019/2020 and () (right): SWE estimates from seNorge and IS2 for Ny-Ålesund in winter 2020/2021

3.5. Available in situ measurements of SWE

In situ measurements of SWE in Svalbard is scarce. A few point measurements are available from Ny Ålesund and Hornsund, and some extended field measurements are also available. These are summarized below.

3.5.1. SWE measurements in Svalbard

Within the SIOS Data Access Portal we were able to find the following datasets that pertains to measurements of snow water equivalent for terrestrial snow (avoiding SWE on sea ice and glaciers).

Table 2. Historical SWE measurements Svalbard

Site	*Sensor*	*Year*	*Research group*
Ny Ålesund	Manual	2019/2020	AWI
Ny Ålesund	Automatic	2019/2020	AWI
Hornsund	Manual	2018-2020	IG PAS
Hornsund	Manual	2022	IG PAS
Grønnfjorden	Manual	2002-2019	U.St.Petersburg

Additionally, we are aware of certain campaigns not yet published as FAIR data under SIOS.

Table 3.GPR based SWE measurements in Svalbard

Site	*Sensor*	*Year*	*Research group*
Ny Ålesund	GPR	2020	NPI
Longyearbyen	GPR	2018-2025	NORCE
Hornsund	GPR	2020-2025	IG PAS

*SWE is here based on snow depth transects and a few density measurements.

3.5.2. SWE measurements in Norway

NORCE has developed an innovative SWE measurement technology based on fibre optic cables integrated in mats that can be deployed over a sufficiently large area to provide representative measurements of SWE for a site comparable with typical satellite image resolutions 100 -500 m^2. The technology is yet not fully operational but has been tested over two winters in mountainous terrain in southern Norway. Two stations have been operated (Vetlebotn and Tyin). The mats have also been compared with traditional large scale snow weights. The preliminary results are quite good for the Vetlebotn site, but the results from the Tyin station (2024/2025) which is close to the LIQUIDICE study site in Jotunheimen were not optimal (Figure 13). The main reason for this was that the current sensor was not sensitive enough for small snow amounts. The instrument is currently being upgraded to increase the sensitivity.

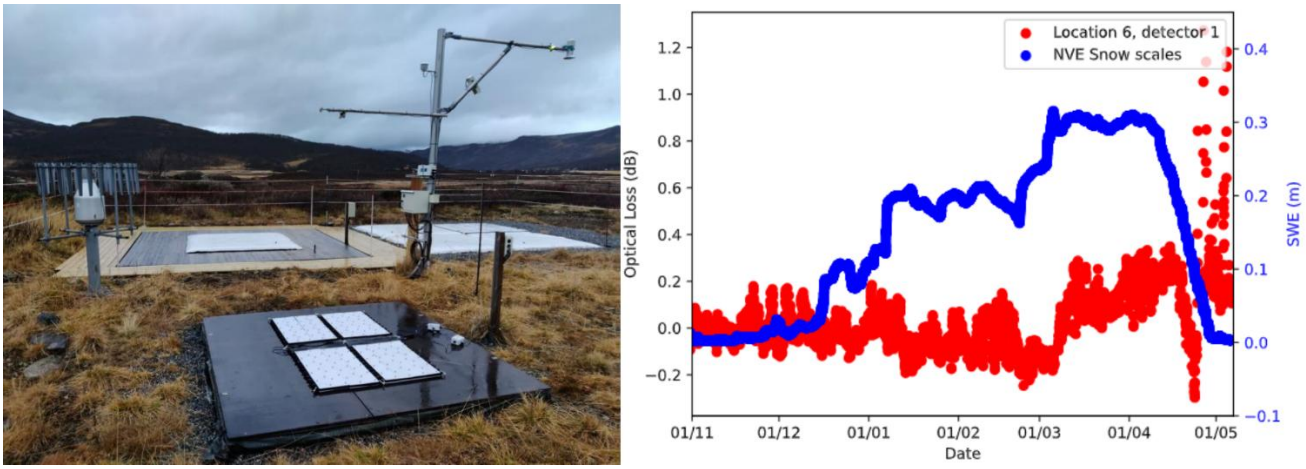

Figure 13. Left: Fibre optic mats mounted on top of traditional snow weights. Right: Signature of fibre optics sensors along with SWE measurements from traditional snow weight.

3.6. Conclusions and outlook

The section gives an overview of available datasets and measurement methods that can be used to validate EO based snow water equivalent datasets. The methods will be used in LIQUIDICE in the following years.

4. Summary

Due to the delay in launch and sub-sequent release of NISAR data, there are currently no new snow water equivalent datasets available for publication in the task 2.2 of LIQUIDICE. NISAR data will become available from mid-march 2026, with a backlog since November 2025, allowing a full investigation of snow water equivalent for several LIQUIDICE study sites.

5. References

Stuefer, S. L., Hale, K., May, L. D., Mason, M., Vuyovich, C., Marshall, H. P.,Dragos V. & Elder, K. (2025). Snow depth measurements from Arctic tundra and boreal forest collected during NASA SnowEx Alaska campaign. Nature Scientific Data, 12(1), 919.

Rott, H., Yueh, S. H., Cline, D. W., Duguay, C., Essery, R., Haas, C., Hélière, F. and Kern, M. and Macelloni, G. and Malnes, E. and Nagler, T., Pulliainen, J., Rebhan, H. and Thompson, A.. (2010). Cold regions hydrology high-resolution observatory for snow and cold land processes. *Proceedings of the IEEE*, *98*(5), 752-765.

Jenssen, R. O. R. and Jacobsen, S. K. Measurement of snow water equivalent using drone-mounted ultra-wide-band radar. Remote Sensing, 13(13), 2610, 2021.

Guneriussen, T., Hogda, K. A., Johnsen, H.,and Lauknes, I. InSAR for estimation of changes in snow water equivalent of dry snow. *IEEE Transactions on Geoscience and Remote Sensing*, *39*(10), 2101-2108, 2001

Leinss, S., Wiesmann, A., Lemmetyinen, J., & Hajnsek, I. Snow water equivalent of dry snow measured by dif-ferential interferometry. IEEE Journal of Selected Topics in Applied Earth Observations and Remote Sensing, 8(8), 3773-3790, 2015.

Funnell, A.C.; Thomas, P.J. Design of a Flexible Weight Sensor Using Optical Fibre Macrobending. Sensors, 23, 912. https://doi.org/10.3390/s23020912, 2023.

Moholdt, G., Wesselink, D., Aas, H.F. (2019). Merged Svalbard digital terrain model [Data set]. Norwegian Polar Institute. https://doi.org/10.21334/npolar.2019.675565f7

Malnes E., Vickers H., Grahn J., Rydeng Jensen R-O, Ricker R. and Lauknes T.R., Multi-frequency synthetic aperture radar observations of avalanches and snow parameters in Svalbard, Proceedings to ISSW24, International Snow Science workshop, Tromsø, Norway. 23-28 sept, 2024.